Stochastic Global Identification of a Bio-inspired Self-sensing Composite UAV Wing via Wind Tunnel Experiments

Fotis Kopsaftopoulos, Raphael Nardari, Yu-Hung Li, Pengchuan Wang, and Fu-Kuo Chang

Department of Aeronautics and Astronautics, Stanford University, Stanford CA 94305, USA

ABSTRACT

In this work, the system design, integration, and wind tunnel experimental evaluation are presented for a bio-inspired self-sensing intelligent composite unmanned aerial vehicle (UAV) wing. A total of 148 micro-sensors, including piezoelectric, strain, and temperature sensors, in the form of stretchable sensor networks are embedded in the layup of a composite wing in order to enable its self-sensing capabilities. Novel stochastic system identification techniques based on time series models and statistical parameter estimation are employed in order to accurately interpret the sensing data and extract real-time information on the coupled airflow-structural dynamics. Special emphasis is given to the wind tunnel experimental assessment under various flight conditions defined by multiple airspeeds and angles of attack. A novel modeling approach based on the recently introduced Vector-dependent Functionally Pooled (VFP) model structure is employed for the stochastic identification of the "global" coupled airflow-structural dynamics of the wing and their correlation with dynamic flutter and stall. The obtained results demonstrate the successful system-level integration and effectiveness of the stochastic identification approach, thus opening new perspectives for the state sensing and awareness capabilities of the next generation of "fly-by-feel" UAVs.

Keywords: bio-inspired systems, composite wing, system identification, sensor networks, stochastic systems, structural health monitoring, piezoelectric sensors, autoregressive models, aerial vehicles, flight awareness

1. INTRODUCTION

The next generation of intelligent aerospace structures and air vehicles will be able to "feel", "think", and "react" in real time based on high-resolution state-sensing capabilities allowing for superior performance in complex dynamic environments, safer operation, reduced maintenance costs, and complete life-cycle monitoring. One of the main challenges of the current state-of-the-art research is the development of technologies that will lead to autonomous "fly-by-feel" unmanned aerial vehicles (UAVs) inspired by the unprecedented sensing and actuation capabilities of biological systems. Such intelligent air vehicles will be able to (i) sense the environment (temperature, ambient air pressure, etc.), (ii) sense their flight (vibration, flutter, stall, aerodynamic loads, etc.) and structural health state (detect, localize and quantify damage), and (iii) effectively interpret the sensing data to achieve real-time state awareness and improve the vehicle performance and control characteristics. However, and despite the importance of vehicle state sensing and awareness, the current state of the art is primitive as well as prohibitively heavy, expensive, and complex. Therefore, a departure from the existing technologies is necessary for the design and deployment of the next generation of intelligent air vehicles.

Self-sensing multifunctional materials are highly intelligent materials that constitute the future generation of composites for aerospace applications.[1–4] Furthermore, a dramatic rise is seen in the application of advanced composite materials for aerospace applications in the last two decades. Industry analysts estimate a growth of 8 to 13 % per year in the carbon fiber reinforced plastics market for the next several years.[5] Towards this end, current research aims at the development of the technologies that will lead to the next generation of self-sensing self-diagnostic composite structures and autonomous aerospace systems that can sense the environment (temperature, pressure, humidity, etc.) and structural state (configuration, loads, damage, etc.), and effectively interpret the sensing data to achieve real-time state awareness under uncertainties in varying operating environments. Such self-sensing composite materials will enable the integration with SHM systems[6–10] in which a network of sensors is attached or embedded inside the composite structure.

Corresponding author: Fotis Kopsaftopoulos; E-mail: fkopsaf@stanford.edu

in the Proceedings of the SPIE Smart Structures and Materials + Nondestructive Evaluation and Health Monitoring, March 2016, Las Vegas, NV, USA

The design, integration, and wind tunnel experimental assessment are presented for an intelligent composite UAV wing with state-sensing and awareness capabilities. The proposed design incorporates novel bio-inspired multi-modal sensor networks that can be embedded inside composite materials to provide built-in sensing and intelligence capabilities to various structural components (wings, fuselage, other critical components). Micro-fabricated stretchable sensor networks, including integrated piezoelectric, strain, and temperature sensors are designed and monolithically embedded in the layup of the composite wing. The self-sensing capabilities of the intelligent composite UAV wing are achieved via four stretchable sensor networks that are embedded inside the carbon/glass fiber composite layup. Each of the four sensor networks fabricated for this work consist of 8 piezo-electric lead-zirconate titanate (PZT) sensors, 6 strain gauges, and 23 resistive temperature detectors (RTDs). The fabricated wing can sense its structural state and surrounding environment during flight and interpret the sensing information in order to determine its actual operating state and flight configuration. Piezoelectric sensors are used to sense the vibration of the wing in order to identify and monitor the coupled airflow-structural dynamics. Strain gauges are used to determine the strain distribution of the wing and identify potential critical areas for the considered experimental conditions. Some preliminary results focusing on the response of the strain gauges and the non-parametric analysis of the piezoelectric response signals have been recently published by the authors[4] and are not considered in this work. However, this is the first time that a stochastic framework for the parametric identification of the "global" wing dynamics is presented.

In this study, special emphasis is given to the wind tunnel experimental assessment under various flight (operating) conditions defined by multiple airspeeds and angles of attack. A novel modeling approach based on the recently introduced Vector-dependent Functionally Pooled (VFP) model structure[11–13] is employed for the stochastic identification of the coupled airflow-structural dynamics for the complete range of the admissible flight conditions; that is all airspeeds and angles of attack that are considered in the wind tunnel experiments and may form the flight envelope of the UAV. The unique characteristic of the VFP-based modeling approach is that it enables the analytical inclusion of *both* the airspeed and angle of attack on the coupled airflow-structural dynamics, as the VFP model parameters depend functionally on the flight conditions. The VFP identification approach leads to the estimation of a compact and accurate "global" model in a statistically optimal sense.

This VFP-based identification framework is based on three important entities:

(i) A stochastic Functionally Pooled (FP) model structure that explicitly allows for system modeling under multiple operating conditions via a single ("global") mathematical representation. This representation is characterized by parameters that functionally (explicitly) depend on the operating parameter in a quasi-static fashion and allows for the proper, parsimonious, modeling of the dynamics under all possible conditions without using excessively many parameters or requiring a separate interpolation stage.

(ii) Data pooling techniques which simultaneously treat, as a single entity, the data records corresponding to all available operating conditions. In this way potential interrelations are also accounted for.

(iii) Properly formulated statistical inference techniques for model estimation.

The rest of the paper is organized as follows: The the bio-inspired stretchable sensor networks and the wing integration are presented in section 2. The wind tunnel experiments are described in section 3, while the VFP-based stochastic identification approach is outlined in section 4. The experimental results are provided in section 5, while the conclusions are summarized in section 6.

2. BIO-INSPIRED SENSOR NETWORKS AND WING INTEGRATION

Recently, micro-fabricated expandable sensor networks have been developed and deployed micro-scale sensors over macroscopic areas.[1–3, 14–17] In order to survive the large strains that occur in expansion, the sensors are created on polymer substrates with nonstandard and unique micro-fabrication processes. The resulting components have dimensions on the order of tens of micrometers (Figure 1).

These networks are created on standard 100 mm diameter substrates and expanded to span areas orders of magnitude larger than the initial fabrication area deploying numerous micro-meter scale devices over meter scale

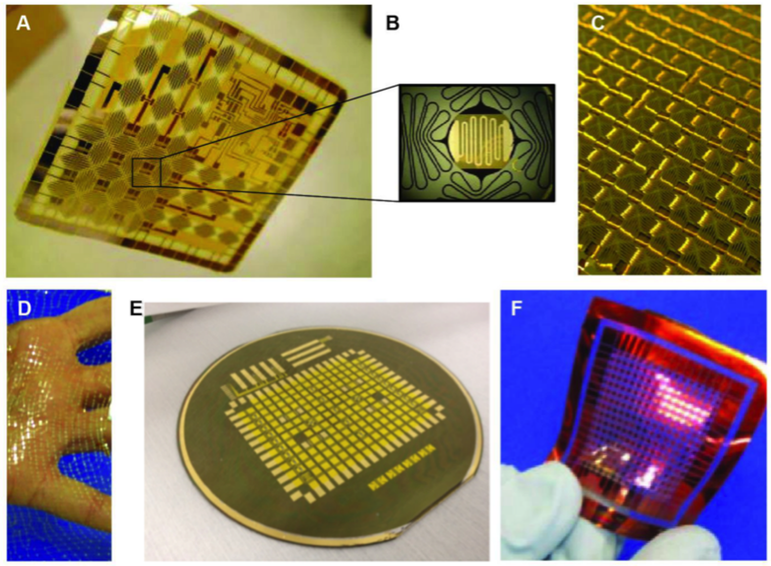

Figure 1. (A) A 16-node sensor network on a wafer can be expanded up to $1,057\%$ in each dimension after release. (B) Close-up of the sensor node demonstrating the design of the microwires. (C) A sensor network with 169 nodes before expansion. (D) An expanded 5041-node network is shown in contrast to a hand, which illustrates the flexibility of the membrane. (E) Network before release on a 4-inch wafer. (F) A fabricated 256-node network on polyimide is easily held by hand without damaging the network. It is characterized by 16 μm wide, 50 μm thick microwires.

areas. The resulting web-like network consists of distributed small scale components (nodes, wires, pads, etc.) intended to have a minimal parasitic effect on the host structure. The component size is on the same order as an individual fiber in typical composite materials or scrim in film adhesives and small enough to be placed into a composite without structural modifications. These networks can be used in-situ, from the material fabrication throughout its service life, to monitor the cure process of composite materials, characterize material properties post-cure, and monitor the structural dynamics along with the health of the structure during its life cycle.

In this work four stretchable sensor networks with integrated distributed PZT, strain, and RTD sensors have been designed and fabricated[1–3,14–16] so that they can be embedded inside the layup of the composite wing. Extensible wires connect the network nodes and serve as the signal communication channels. Before stretching, the network dimensions are 52.8 mm by 39.6 mm that after the stretching process expand to 140 mm by 105 mm yielding a 700% total surface area increase.[16] Each of the four sensor networks contains 8 piezoelectric sensors (round PZTs 3.175 mm in diameter), 6 strain gauges, and 24 RTDs. The total number of embedded sensors in the composite wing is 148.

2.1 The Intelligent Composite Wing

The prototype wing was designed, constructed and tested at Stanford University. The designed wing is based on the cambered SG6043 high lift-to-drag ration airfoil with a 0.86 m wing span, 0.235 m chord, and an aspect ratio of 3.66. In order to achieve the successful integration and fabrication of the wing prototype, an appropriate network-material integration process had to be developed for embedding the micro-fabricated sensor networks inside the composite materials.

The micro-scale, aspect ratio, and fragile nature of the stretchable network components, including both the wires and the sensor nodes, requires the use of appropriate integration and network transfer processes. The geometry and material of the network nodes and contact pads may cause the electrical shorting with the carbon fibers if not properly addressed. In order to tackle these integration and manufacturing challenges, a new process had to be developed for the transfer, electrical interfacing and electrical insulation of the network components based on multilayer flexible PCB technologies and epoxy armoring. Via the use of the developed approach the sensor networks were successfully integrated into carbon fiber based composite materials using a multi-step

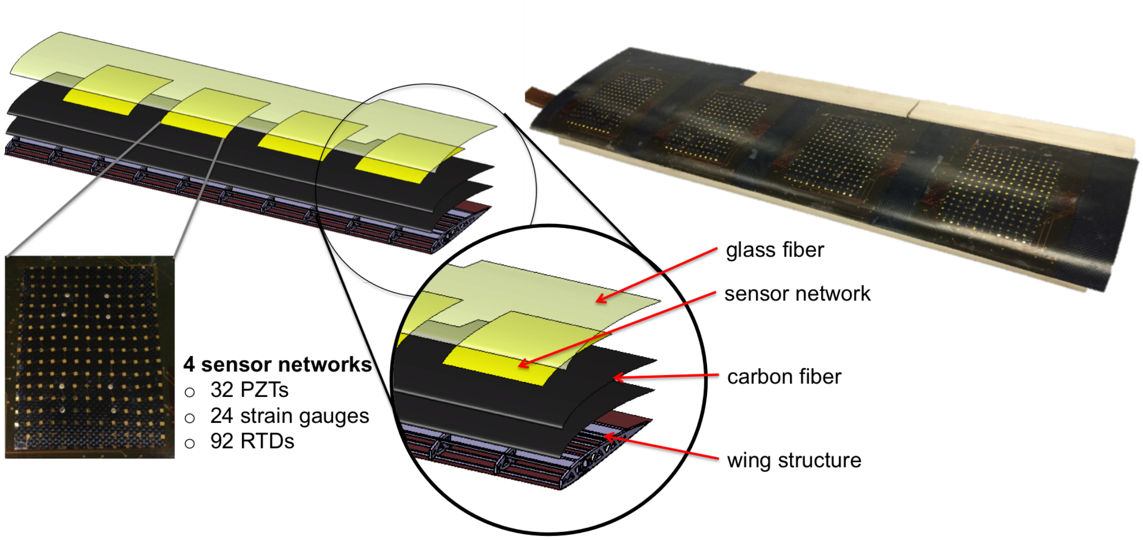

Figure 2. The intelligent composite wing design with a total of 148 (32 piezoelectric, 24 strain gauges, and 92 RTDs) micro-sensors embedded in the composite layup.

fabrication process. The composite wing structure was manufactured based on carbon and glass laminated composites. The layup consists of carbon fiber (CF) plain wave fabric 1K T300 and glass fiber (GF) plain wave fabric 18 gr/m^2 infused with Araldite LY/HY5052 epoxy. The stacking sequence of the layers was [0^o GF, 0^o CF, 45^o CF, 45^o CF, 0^o CF, 0^o GF] (Figure 2).

The four networks were embedded between the two top layers at 0^o of the layup (near the wing surface) during the lamination process. The glass fiber was employed due to its transparency, so that the embedded stretchable sensor networks may be evident to the naked eye. The supporting wing structure consists of wooden (basswood) ribs and spars.

3. WIND TUNNEL EXPERIMENTS

3.1 The Wind Tunnel

The prototype composite wing was tested in the open-loop wind tunnel facility at Stanford University. The wind tunnel has a square test section of 0.76 m by 0.76 m (30 by 30 in) and can achieve continuous flow speeds up to approximately 40 m/s. A custom basis was designed and fabricated to support the wing and permit adjustments in the angle of attack. The wing was mounted horizontally inside the test section. Eight commercial strain gauges were attached on appropriate locations of the basis to measure the aerodynamic forces. The axis of rotation coincided approximately with the quarter of the wing chord. Figure 3 presents the composite wing with the corresponding locations of the PZTs and strain sensors. Table 1 presents the wing dimensions.

Table 1. Wing dimensions.

Chord c	0.235 m
Span b	0.86 m
Area S	0.2 m^2
Aspect Ratio AR	3.66

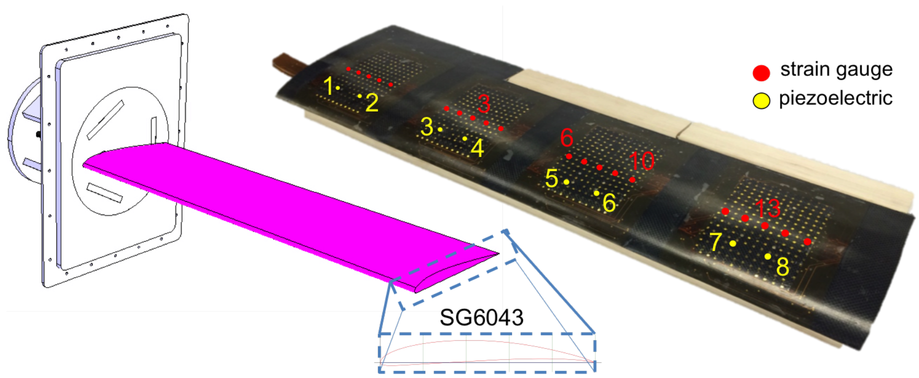

Figure 3. The intelligent composite wing with the embedded sensor networks and the locations of the piezoelectric and strain sensors.

3.2 The Experiments

A series of wind tunnel experiments were conducted for various angles of attack and free-stream velocities U_∞. For each angle of attack, from 0 degrees up to 18 degrees with an incremental step of 1 degree, data were sequentially collected for velocities from 9 m/s up to 22 m/s (incremental step 1 m/s). The above procedure resulted in 285 different experiments covering the complete range of the considered experimental conditions. The experimental conditions along with the Reynolds numbers are outlined in Table 2.

For each experiment the vibration and strain responses were recorded at different locations on the wing via the embedded network piezoelectric sensors (initial sampling frequency $f_s = 1000$ Hz, initial signal bandwidth $0.1 - 500$ Hz) and strain gauges (sampling frequency $f_s = 100$ Hz, signal bandwidth DC100 Hz), respectively. The strain signals were driven through a custom designed and built signal conditioning device into the data acquisition system (National Instruments). The total number of the sensor signals that were obtained was limited by the available number of channels of the data acquisition system. Table 3 presents the sensors, data acquisition, signal details.

4. STOCHASTIC IDENTIFICATION UNDER MULTIPLE FLIGHT CONDITIONS

In this section the identification of the coupled airflow-structural dynamics is presented via the use of stochastic functional models, or more precisely Vector-dependent Functionally Pooled AutoRegressive (VFP-AR) models. These models are capable of representing the system dynamics for the complete range of operating (flight) conditions (airspeeds and angle of attack). The identification of stochastic systems operating under multiple conditions is addressed based on data records obtained under a sample of these conditions. The problem is important in a number of practical applications and is tackled within a recently introduced Functional Pooling

Table 2. The conditions considered in the wind tunnel experiments.

Re ($\times 10^3$)	124	155	171	187	202	217	233	248	264	280	295	311	326	342
U_∞ (m/s)	9	10	11	12	13	14	15	16	17	18	19	20	21	22
Angle of attack: $0 - 18$ degrees; Total number of experiments: 266														

Table 3. Signal pre-processing and details.

	Piezoelectric sensors	**Strain gauges**
Number of sensors:	8	15
Sampling frequency:	$f_s = 1000$ Hz	$f_s = 100$ Hz
Bandwidth:	$[0.1 - 500]$ Hz	$[DC - 50]$ Hz
Signal length:	$N = 90,000$ samples (90 s)	$N = 9,000$ samples (90 s)

framework.[11–13] This study focuses on the case of operating conditions characterized by two parameters, namely the airspeed and the angle of attack of the wing.

Classical system identification aims at deriving a model representing a system under a specific operating condition. Yet, in many cases, a system may operate under different conditions at different occasions (time periods), with the dynamics depending in a pseudo-static fashion on certain operating parameter(s) - also referred to as scheduling parameter(s). In such cases, given a number of data records from the system operating under a sample of different conditions, it is highly desirable to establish a single and global model, that, while compact (parsimonious), will be capable of accurately representing the dynamics under any considered condition.

4.1 Baseline Modeling Under a Single Operating Condition

The modeling of the wing under a single operating condition is an initial step performed in order to facilitate (in the sense of providing approximate model orders) the subsequent step of the global modeling under all the admissible operating conditions.

A single experiment is performed, based on which an interval estimate of a discrete-time model (or a vector model or an array of models in the case of several vibration response measurement locations) representing the system dynamics is obtained via standard identification procedures.[18,19] In this study a single response AutoRegressive (AR) model is used.

An AR(n) model is of the form[*]:[18]

$$y[t] + \sum_{i=1}^{n} a_i \cdot y[t-i] = e[t] \qquad e[t] \sim \text{iid}\,\mathcal{N}\big(0, \sigma_e^2\big) \tag{1}$$

with t designating the normalized discrete time ($t = 1, 2, 3, \ldots$ with absolute time being $(t-1)T_s$, where T_s stands for the sampling period), $y[t]$ the measured vibration response signals as generated by the piezoelectric sensors of the wing, n the AR order, and $e[t]$ the stochastic model residual (one-step-ahead prediction error) sequence, that is a white (serially uncorrelated), Gaussian, zero mean with variance σ_e^2 sequence. The symbol $\mathcal{N}(\cdot,\cdot)$ designates Gaussian distribution with the indicated mean and variance, and iid stands for identically independently distributed.

The model is parameterized in terms of the parameter vector $\bar{\boldsymbol{\theta}} = [a_1 \ \ldots \ a_n \ \vdots \ \sigma_e^2]^T$ to be estimated from the measured signals.[18] Model estimation may be achieved based on minimization of the Ordinary Least Squares (OLS) or the Weighted Least Squares (WLS) criteria.[18] The modeling procedure involves the successive fitting of AR(n) models for increasing order n until an adequate model is selected.[20] Model order selection is based on the Bayesian Information Criterion (BIC) and the residual sum of squares normalized by the series sum of squares (RSS/SSS). Final model validation is based on formal verification of the residual (one-step-ahead prediction error) sequence uncorrelatedness (whiteness) hypothesis [18, pp. 512-513].

4.2 Global Modeling Under Multiple Operating Conditions

The VFP-AR representation allows for complete and precise modeling of the global wing dynamics under multiple operating conditions defined by varying airspeed and angle of attack. The VFP model parameters and residual series covariance depend functionally on the airspeed and angle of attack, while the corresponding interrelations and statistical dependencies between the different operating conditions are taken into account.

The VFP-AR representation belongs to the recently introduced broader class of stochastic FP models, which make use of data pooling techniques for combining and optimally treating (as one entity) the data obtained from various experiments corresponding to different structural states and statistical techniques for model estimation.[12,13]

The global modeling of the composite wing via a VFP-AR model involves consideration of all the admissible airspeeds and angles of attack that define the flight envelope of the wing. A total of $M_1 \times M_2$ experiments is performed (physically or via analytical models and simulations), with M_1 and M_2 designating the number of

[*]Lower case/capital bold face symbols designate vector/matrix quantities, respectively.

experiments under the various airspeeds and angles of attack, respectively. Each experiment is characterized by a specific airspeed k^1 and a specific angle of attack k^2, with the complete series covering the required range of each variable, say $[k^1_{min},\, k^1_{max}]$ and $[k^2_{min},\, k^2_{max}]$, via the discretizations $\{k^1_1, k^1_2, \ldots, k^1_{M_1}\}$ and $\{k^2_1, k^2_2, \ldots, k^2_{M_2}\}$. For the identification of a global VFP model the vector operating parameter $\boldsymbol{k}$ containing the airspeed and angle of attack components, is defined as:

$$\boldsymbol{k} = [k^1_i\ k^2_j]^T \Longleftrightarrow k_{i,j}, \quad i = 1, \ldots, M_1, \quad j = 1, \ldots, M_2 \tag{2}$$

with $k_{i,j}$ designating the flight state of the wing corresponding to the i-th airspeed and the j-th angle of attack. This procedure yields a pool of response signals (each of length N):

$$x_{\boldsymbol{k}}[t], y_{\boldsymbol{k}}[t] \ \text{ with } t = 1, \ldots, N,\ k^1 \in \{k^1_1, \ldots, k^1_{M_1}\},\ k^2 \in \{k^2_1, \ldots, k^2_{M_2}\}. \tag{3}$$

A proper mathematical description of the wing structure may be then obtained in the form of a VFP-AR model. In the case of several vibration measurement locations an array of such models (or else a vector model) may be obtained, with each scalar model corresponding to each measurement location.

The VFP-AR model is of the following form:[12]

$$y_{\boldsymbol{k}}[t] + \sum_{i=1}^{n} a_i(\boldsymbol{k}) \cdot y_{\boldsymbol{k}}[t-i] = e_{\boldsymbol{k}}[t] \tag{4a}$$

$$e_{\boldsymbol{k}}[t] \sim \text{ iid}\, \mathcal{N}\big(0, \sigma_e^2(\boldsymbol{k})\big) \qquad \boldsymbol{k} \in \mathbb{R}^2 \tag{4b}$$

$$a_i(\boldsymbol{k}) = \sum_{j=1}^{p} a_{i,j} \cdot G_j(\boldsymbol{k}) \tag{4c}$$

$$E\{e_{k_{i,j}}[t] \cdot e_{k_{m,n}}[t-\tau]\} = \gamma_e[k_{i,j}, k_{m,n}] \cdot \delta[\tau] \tag{4d}$$

with n designating the AR order, $y_{\boldsymbol{k}}[t]$ the piezoelectric sensor's response signal, and $e_{\boldsymbol{k}}[t]$ the model's residual (one-step-ahead prediction error) sequence, that is a white (serially uncorrelated) zero mean sequence with variance $\sigma_e^2(\boldsymbol{k})$. This may potentially be cross-correlated with its counterparts corresponding to different experiments (different $\boldsymbol{k}$'s). The symbol $E\{\cdot\}$ designates statistical expectation, $\delta[\tau]$ the Kronecker delta (equal to unity for $\tau = 0$ and equal to zero for $\tau \neq 0$), $\mathcal{N}(\cdot,\cdot)$ Gaussian distribution with the indicated mean and variance, and iid stands for identically independently distributed.

As (4c) indicates, the AR parameters $a_i(\boldsymbol{k})$ are modeled as explicit functions of the vector $\boldsymbol{k}$ (which contains the airspeed and angle of attack components) by belonging to p-dimensional functional subspace spanned by the mutually independent basis functions $G_1(\boldsymbol{k}), G_2(\boldsymbol{k}), \ldots, G_p(\boldsymbol{k})$ (*functional basis*). The functional basis consists of polynomials of two variables (bivariate) obtained as tensor products from their corresponding univariate polynomials (Chebyshev, Legendre, Jacobi, and other families[11,12]). The constants $a_{i,j}$ designate the AR coefficients of projection.

The VFP-AR model of (4a)–(4d) is parameterized in terms of the parameter vector to be estimated from the measured signals:

$$\bar{\boldsymbol{\theta}} = [\ a_{1,1}\ a_{1,2}\ \ldots\ a_{i,j} \ \vdots\ \sigma_e^2(\boldsymbol{k})\ ]^T \quad \forall\, \boldsymbol{k} \tag{5}$$

and may be written in linear regression form as:

$$y_{\boldsymbol{k}}[t] = \big[\boldsymbol{\varphi}^T_{\boldsymbol{k}}[t] \otimes \boldsymbol{g}^T(\boldsymbol{k})\big] \cdot \boldsymbol{\theta} + e_{\boldsymbol{k}}[t] = \boldsymbol{\phi}^T_{\boldsymbol{k}}[t] \cdot \boldsymbol{\theta} + e_{\boldsymbol{k}}[t] \tag{6}$$

with:

$$\begin{aligned}
\boldsymbol{\varphi}_{\boldsymbol{k}}[t] \quad &:= \quad \Big[-y_{\boldsymbol{k}}[t-1] \ \ldots \ -y_{\boldsymbol{k}}[t-n]\Big]^T_{[n\times 1]} && \text{(7a)}\\
\boldsymbol{g}(\boldsymbol{k}) \quad &:= \quad \Big[G_1(\boldsymbol{k}) \ \ldots \ G_p(\boldsymbol{k})\Big]^T_{[p\times 1]} && \text{(7b)}\\
\boldsymbol{\theta} \quad &:= \quad \Big[a_{1,1} \ a_{1,2} \ \ldots \ a_{n,p}\Big]^T_{[(np\times 1]} && \text{(7c)}
\end{aligned}$$

and ^{T} designating transposition and $\otimes$ Kronecker product [21, Chap. 7].

Pooling together the expressions (6) of the VFP-AR model corresponding to all vector operating parameters $\boldsymbol{k}$ $(k_{1,1}, k_{1,2}, \ldots, k_{M_1,M_2})$ considered in the experiments (cross-sectional pooling) yields:

$$\begin{bmatrix} y_{k_{1,1}}[t] \\ \vdots \\ y_{k_{M_1,M_2}}[t] \end{bmatrix} = \begin{bmatrix} \phi^T_{k_{1,1}}[t] \\ \vdots \\ \phi^T_{k_{M_1,M_2}}[t] \end{bmatrix} \cdot \boldsymbol{\theta} + \begin{bmatrix} e_{k_{1,1}}[t] \\ \vdots \\ e_{k_{M_1,M_2}}[t] \end{bmatrix} \Longrightarrow \boldsymbol{y}[t] = \boldsymbol{\Phi}[t] \cdot \boldsymbol{\theta} + \boldsymbol{e}[t]. \tag{8}$$

Then, following substitution of the data for $t = 1, \ldots, N$ the following expression is obtained:

$$\boldsymbol{y} = \boldsymbol{\Phi} \cdot \boldsymbol{\theta} + \boldsymbol{e} \tag{9}$$

with

$$\boldsymbol{y} := \begin{bmatrix} \boldsymbol{y}[1] \\ \vdots \\ \boldsymbol{y}[N] \end{bmatrix}, \quad \boldsymbol{\Phi} := \begin{bmatrix} \boldsymbol{\Phi}[1] \\ \vdots \\ \boldsymbol{\Phi}[N] \end{bmatrix}, \quad \boldsymbol{e} := \begin{bmatrix} \boldsymbol{e}[1] \\ \vdots \\ \boldsymbol{e}[N] \end{bmatrix}. \tag{10}$$

Using the above linear regression framework the simplest approach for estimating the projection coefficient vector $\boldsymbol{\theta}$ is based on minimization of the Ordinary Least Squares (OLS) criterion $J^{\text{OLS}} := \frac{1}{N}\sum_{t=1}^{N} \boldsymbol{e}^T[t]\boldsymbol{e}[t]$.

A more appropriate criterion is (in view of the Gauss-Markov theorem[22]) the Weighted Least Squares (WLS) criterion:

$$J^{\text{WLS}} := \frac{1}{N}\sum_{t=1}^{N} \boldsymbol{e}^T[t]\boldsymbol{\Gamma}^{-1}_{\boldsymbol{e}[t]}\boldsymbol{e}[t] = \frac{1}{N}\boldsymbol{e}^T\boldsymbol{\Gamma}^{-1}_{\boldsymbol{e}}\boldsymbol{e} \tag{11}$$

which leads to the *Weighted Least Squares (WLS)* estimator:

$$\widehat{\boldsymbol{\theta}}^{\text{WLS}} = \left[\boldsymbol{\Phi}^T\boldsymbol{\Gamma}^{-1}_{\boldsymbol{e}}\boldsymbol{\Phi}\right]^{-1}\left[\boldsymbol{\Phi}^T\boldsymbol{\Gamma}^{-1}_{\boldsymbol{e}}\boldsymbol{y}\right]. \tag{12}$$

In these expressions $\boldsymbol{\Gamma}_{\boldsymbol{e}} = E\{\boldsymbol{e}\boldsymbol{e}^T\}$ ($\boldsymbol{\Gamma}_{\boldsymbol{e}} = \boldsymbol{\Gamma}_{\boldsymbol{e}[t]} \otimes \boldsymbol{I}_N$, with $\boldsymbol{I}_N$ designating the $N \times N$ unity matrix) designates the residual covariance matrix, which is practically unavailable. Nevertheless, it may be consistently estimated by applying (in an initial step) Ordinary Least Squares (details in[12]). Once $\widehat{\boldsymbol{\theta}}^{\text{WLS}}$ has been obtained, the final residual variance and residual covariance matrix estimates are obtained as:

$$\widehat{\sigma}^2_e(\boldsymbol{k}, \widehat{\boldsymbol{\theta}}^{\text{WLS}}) = \frac{1}{N}\sum_{t=1}^{N} e^2_{\boldsymbol{k}}[t, \widehat{\boldsymbol{\theta}}^{\text{WLS}}], \quad \widehat{\boldsymbol{\Gamma}}_{\boldsymbol{e}[t]} = \frac{1}{N}\sum_{t=1}^{N} \boldsymbol{e}[t, \widehat{\boldsymbol{\theta}}^{\text{WLS}}]\boldsymbol{e}^T[t, \widehat{\boldsymbol{\theta}}^{\text{WLS}}]. \tag{13}$$

The estimator $\widehat{\boldsymbol{\theta}}^{\text{WLS}}$ may, under mild conditions, be shown to be asymptotically Gaussian distributed with mean coinciding with the true parameter vector $\boldsymbol{\theta}^o$ and covariance matrix $\boldsymbol{P}_{\boldsymbol{\theta}}$:

$$\sqrt{N}(\widehat{\boldsymbol{\theta}}_N - \boldsymbol{\theta}^o) \ \sim \ \mathcal{N}(\boldsymbol{0}, \boldsymbol{P}_{\boldsymbol{\theta}}) \quad (N \longrightarrow \infty) \tag{14}$$

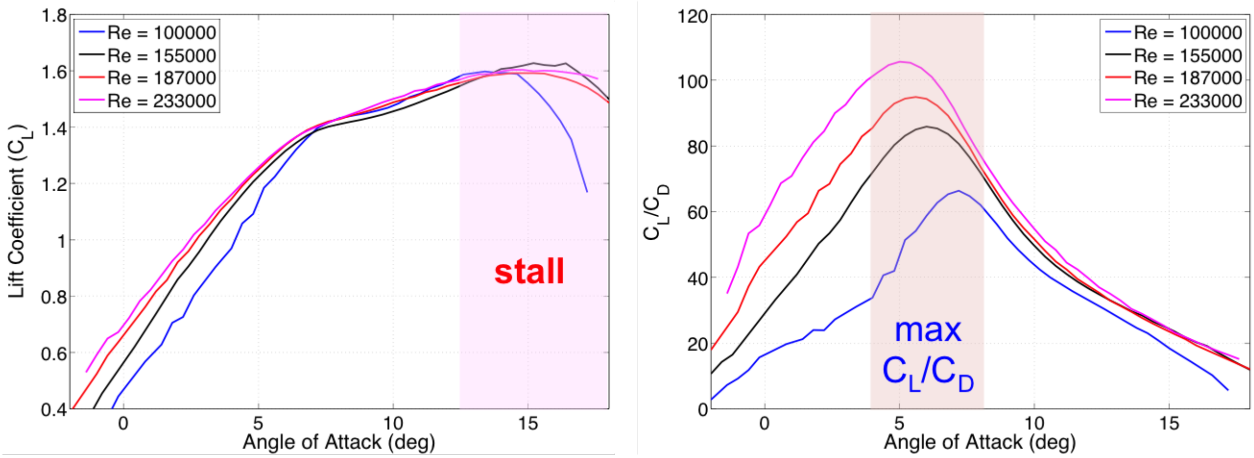

Figure 4. Indicative simulation results: (a) lift coefficient C_L (left subplot) and (b) lift-to-drag coefficient ratio C_L/C_D (right subplot) versus angle of attack for the SG6043 airfoil and various Reynolds numbers.

based on which interval estimates of the true parameter vector may be constructed.[12]

The problem of VFP-AR model structure selection (structure estimation) for a given basis function family (such as Chebyshev, Legendre, and so on), that is model order determination for the AR polynomial and determination of their corresponding functional subspaces, is referred to as the model identification problem. Usually, the AR model order is initially selected via customary model order selection techniques (BIC, RSS, frequency stabilization diagrams),[18] whereas the functional subspace dimensionality is selected via a Genetic Algorithm (GA) procedure.[12] Initially, the maximum functional subspace dimensionality is selected, which defines the search space of the functional subspace estimation subproblem. The determination of the exact subspace dimensionality is achieved via the use of GAs based on minimization of the BIC with respect to the candidate basis functions. In the current study, the estimation of the functional subspace dimensionality was achieved via the use of the BIC criterion for increasing functional subspace dimensionality.

5. EXPERIMENTAL RESULTS

5.1 Numerical Simulations

In order to extract the aerodynamic properties of the fabricated wing based on which the experimental results will be interpreted and assessed, a series of numerical simulations were conducted using the XFOIL, an interactive program for the design and analysis of subsonic isolated airfoils developed at MIT.[23] Given the coordinates specifying the shape of the 2D airfoil, Reynolds number and free stream velocity XFOIL can calculate the pressure distribution on the airfoil and hence lift and drag characteristics.

Figure 4a and Figure 4b present the lift coefficient versus the angle of attack and lift to drag coefficient ratio C_L/C_D results of the SG6043 airfoil of the wing, respectively, for various Reynolds numbers ($U_\infty = 7$, 10, 12 and 15 m/s). It may be readily observed that the wing exhibits stall (loss of lift shown as shaded area in Figure 4a) starting from an angle of attack of approximately 12 degrees for a Reynolds number of $Re = 100,000$. Moreover, observe that the maximum C_L/C_D ratio is obtained for angles between 4 and 8 degrees (shaded areas in Figure 4b).

Figure 5 presents indicative signals obtained from piezoelectric sensor 1 (see Figure 3) under various angles of attack and free stream velocities of $U_\infty = 11$ m/s and $U_\infty = 15$ m/s (see Table 2). Observe the random (stochastic) nature of these signals, which is due to the wind tunnel airflow actuation and the fluid-structure interaction. In addition, it is evident that for higher angles of attack and as the wing approaches stall the signal amplitude (voltage) increases.

Figure 6 presents indicative signal energy ($\text{volt}^2 \cdot t$) results obtained from piezoelectric sensor 1 during the wind tunnel experiments. The angle of attack varied between 0 and 15 degrees with a constant free stream velocity of

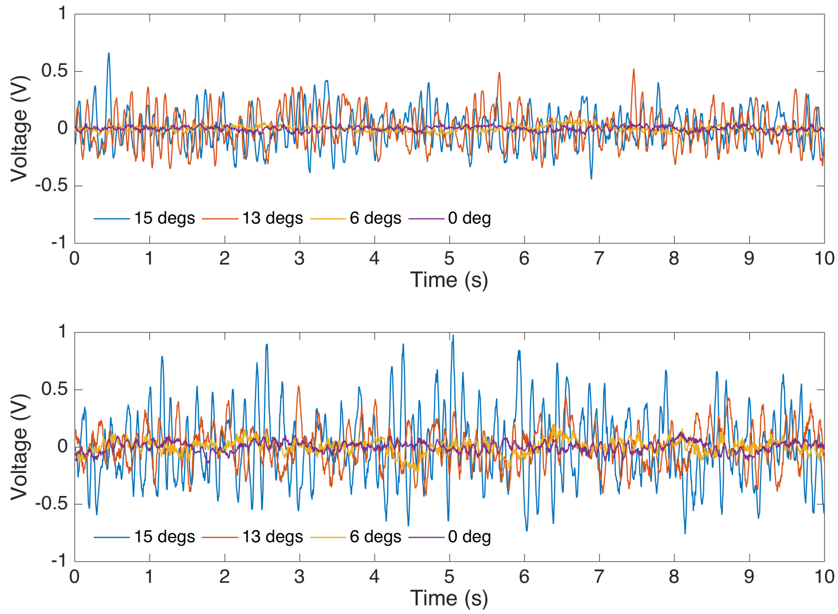

Figure 5. Indicative signals obtained from piezoelectric sensor 1 under various angles of attack: (a) free stream velocity $U_\infty = 11$ m/s (top subplot) and (b) free stream velocity $U_\infty = 15$ m/s (bottom subplot).

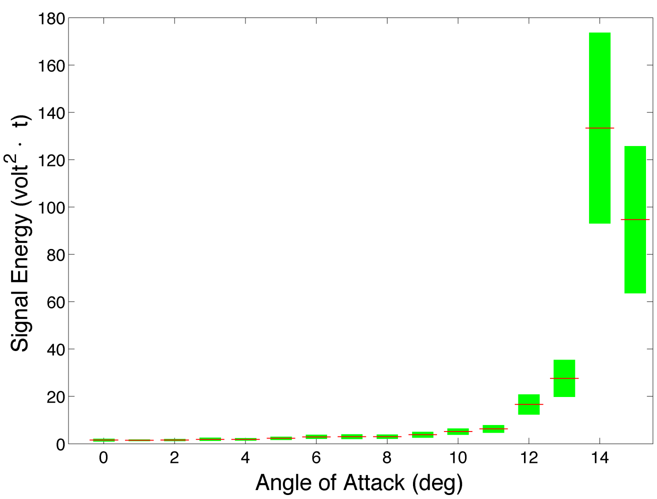

Figure 6. Indicative wind tunnel signal energy versus angle of attack results for piezoelectric sensor 1 and free stream velocity $U_\infty = 15$ m/s. The mean value of the signal energy is shown as red line. The 99% confidence bounds are shown as green shaded areas.

$U_\infty = 15$ m/s. The goal is to correlate the signal energy in the time domain with the airflow characteristics, the structural dynamics, and aeroelastic properties in order to identify and track appropriate signal features that can be used for the airflow and wing vibration monitoring, the localization of the flow separation over the wing chord, and the early detection of stall under various flight and environmental conditions. Figure 6 presents the mean value of the vibrational signal energy along with the 99% confidence bounds. The initial signal of 90 s ($N = 90,000$ samples) was split in signal windows of 0.5 s ($N = 500$ samples). Then, for each signal window the mean value and the standard deviation of the signal energy were calculated.

As the wing angle exceeds the value of 12 degrees the signal energy significantly increases and reaches the

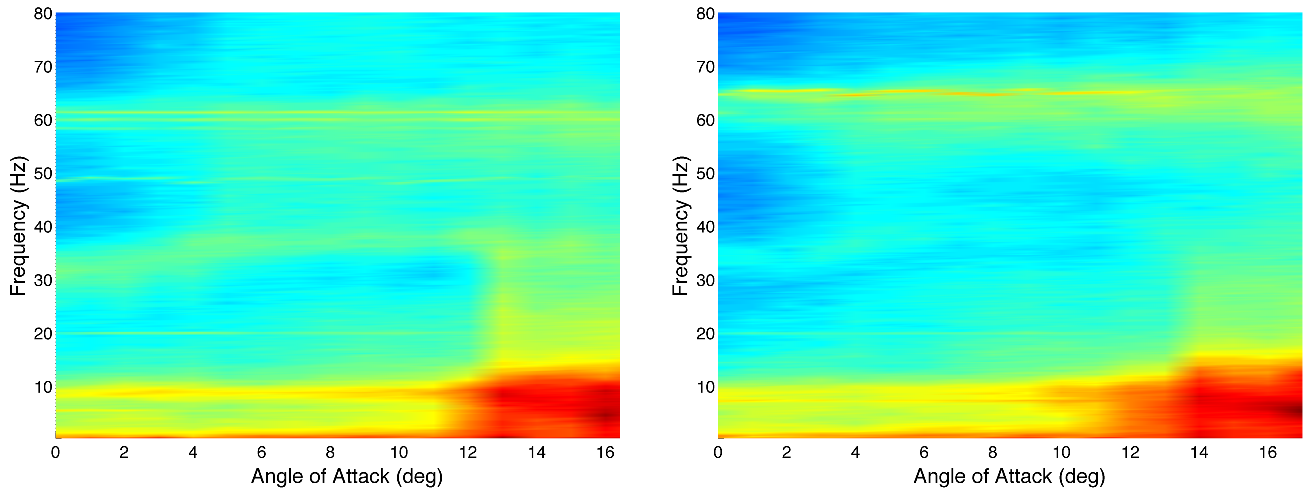

Figure 7. Indicative non-parametric Welch-based PSD estimates (piezoelectric sensor 1) versus angle of attack for (a) $U_\infty = 11$ m/s ($Re = 171,000$; left subplot) and (b) $U_\infty = 15$ m/s ($Re = 233,000$; right subplot) free stream velocities.

maximum value as it approaches the stall range (14 degrees), while slightly decreases after stall has occurred (15 degrees). The wind tunnel results indicated that for the velocities of 11 m/s and 12 m/s the stall angle is 13 degrees, whereas for the higher velocities of 14 m/s and 15 m/s the stall angle appears at 14 degrees. These results are in agreement with the trend of signals in Figure 5 as in both cases the signal amplitude/energy is maximized within the stall range of the wing. Also, the results are in agreement with the numerical simulations presented in Figure 4.

5.2 Non-parametric Analysis

Non-parametric identification is based on $90,000$ (90 s) sample-long response signals obtained from the embedded piezoelectric sensors (see Table 3. A 5096 sample-long Hamming data window (frequency resolution $\Delta f = 0.24$ Hz) with 90% overlap is used for the Welch-based spectral estimation (MATLAB function *pwelch.m*).

Figure 7 presents indicative power spectral density (PSD) Welch-based estimates of the piezoelectric response signals obtained from sensor 1 for increasing angle of attack and free stream velocities $U_\infty = 11$ m/s ($Re = 171,000$) and $U_\infty = 15$ m/s ($Re = 233,000$). Notice that as the angle of attack increases the PSD amplitude in the lower frequency range of [112] Hz significantly increases as well. More specifically, as the angle of the wing approaches the critical stall range of 13 to 14 degrees, depending on the velocity, the low frequency vibrations become dominant and thus indicating the proximity to the stall of the wing. Form this Figure it is evident that by monitoring the identified lower frequency bandwidths that are sensitive to increasing angle of attack we may have a strong indication of stall. All the embedded piezoelectric sensors of the wing exhibit a similar performance, but for the sake of brevity the results are presently omitted.

5.3 Baseline Parametric Modeling

Conventional AR models representing the wing are obtained through standard identification procedures[18,20] based on the collected piezoelectric response signals (MATLAB function *arx.m*). The response signal bandwidth is selected as $0.1 - 100$ Hz after the initial signals were low-pass filtered (Chebyshev Type II) and sub-sampled to a resulting sampling frequency $f_s = 200$ Hz (initial sampling frequency was at 1000 Hz). Each signal resulted in a length of $N = 4,000$ samples (20 s) and was subsequently sample mean corrected (Table 4). For piezoelectric sensor 1, this leads to an AR(72) model for a collected data set corresponding to an airspeed of 11 m/s and an angle of attack of 3 degrees. This model is used as reference and for providing approximate orders for the identification of the global VFP-AR models of the next section. For the sake of brevity, in the following sections indicative results from sensor 1 only will be presented.

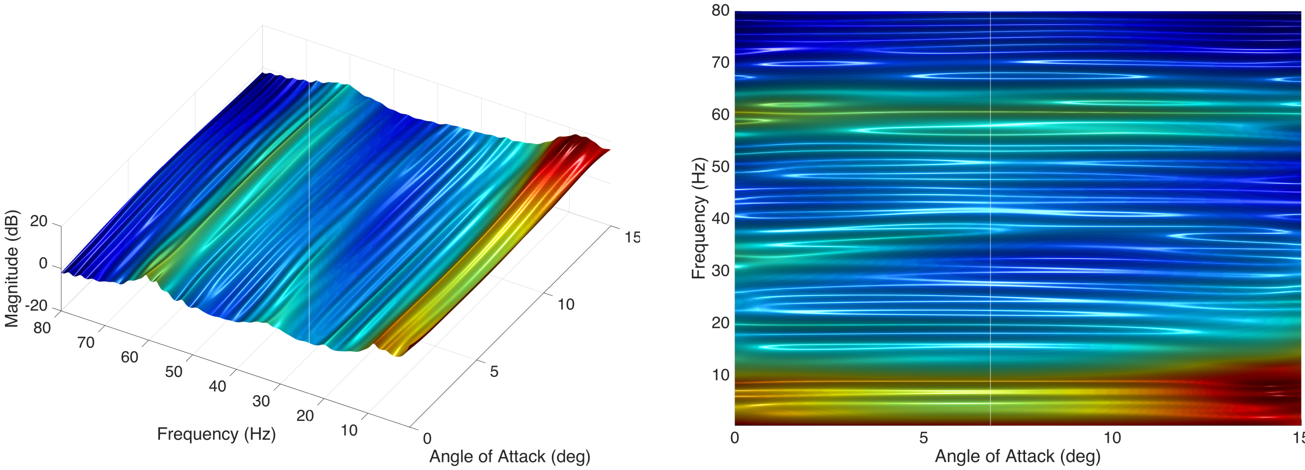

Figure 8. Indicative parametric results obtained from the VFP-AR$(72)_{24}$ model (set airspeed $k^1 = 13$ m/s): spectral amplitude as function of frequency and angle of attack.

5.4 Global Modeling Under Multiple Flight Conditions

The parametric VFP-based identification of the coupled airflow-structural dynamics is based on signals collected from the piezoelectric sensors under the various wind tunnel experiments (see Table 2).

The global modeling of the composite wing is based on signals obtained from a total of $M_1 \times M_2 = 144$ experiments. Airspeeds up to 17 m/s and angles of attack up to 15 degrees were currently considered for the VFP-based modeling procedure. The airspeed and angle of attack increments used are $\delta k^1 = 1$ m/s and $\delta k^2 = 1$ degree, respectively, covering the intervals $[9, 17]$ m/s and $[0, 15]$ degrees.

Model order selection starts with the orders selected for the conventional AR models representing the wing structure for a constant indicative experimental condition. The final model orders being presently selected are based on the BIC criterion[20] and model validation techniques, such as checking the whiteness (uncorrelatedness) and the normality of the model residuals (MATLAB functions *acf.m* and *normplot.m*, respectively).[18,20] The functional subspaces are selected via a similar BIC-based process. The functional subspace consists of 24 Chebyshev Type II bivariate polynomial basis functions.[11,12,24]

The final identified global model is a VFP-AR$(72)_{24}$. The functional subspace consists of the first $p = 24$ shifted Chebyshev Type II 2-dimensional polynomials. Indicative VFP-based spectral results obtained from the VFP-AR$(72)_{24}$ model (for set airspeed $k^1 = 13$ m/s) are, as functions of frequency and angle of attack, depicted in Figure 8. By observing the frequency evolution versus the angle of attack it may be assessed that the amplitude of the parametric power spectral density increases for lower frequencies with the increase of the angle of attack (compare with the non-parametric analysis of Figure 7).

Indicative parametric spectral results obtained from the VFP-AR$(72)_{24}$ model (for set angle of attack $k^2 = 0$ degrees) are, as functions of frequency and airspeed, depicted in Figure 9. Figure 9 presents a close-up of the $0.1 - 30$ Hz frequency range for increasing airspeed. In this case observe how the wing mode at 4.5 Hz for 9 m/s gradually increases with the increasing airspeed until unified with the mode at 8.5 Hz at 16 m/s. This behavior of the wing modes as identified with the VFP-AR model corresponds to the generation of the dynamic flutter

Table 4. Piezoelectric signal pre-processing for the parametric identification.

Sampling frequency:	$f_s = 200$ Hz (after filtering and subsampling)
Final bandwidth:	$[0.1 - 100]$ Hz
Digital filtering:	Low-pass Chebyshev Type II (7th order)
Signal length:	$N = 4,000$ samples (20 s)

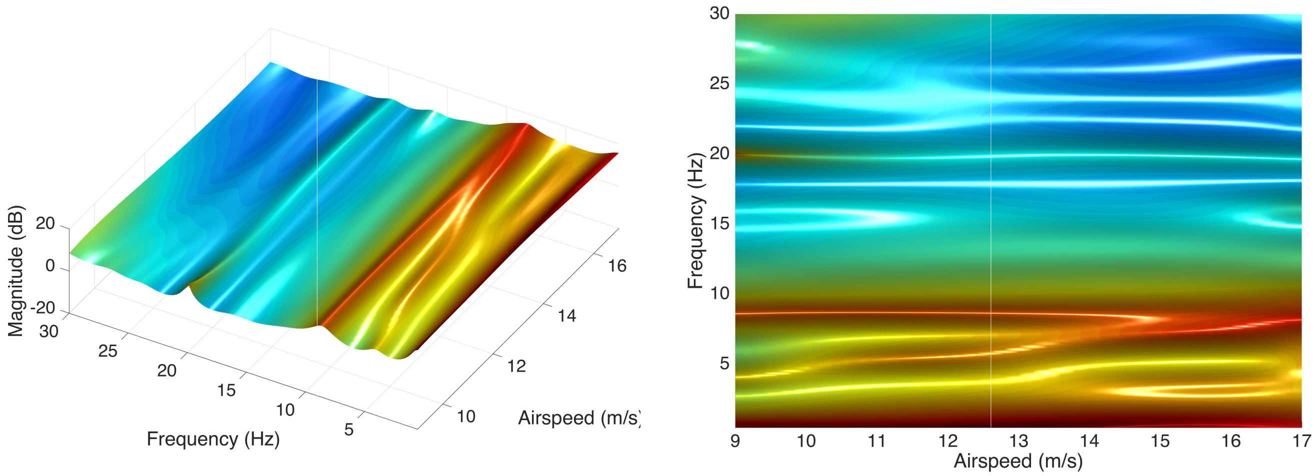

Figure 9. Indicative parametric spectral results obtained from the VFP-AR$(72)_{24}$ model (set angle of attack $k^2 = 0$ degrees): spectral amplitude as function of frequency and airspeed.

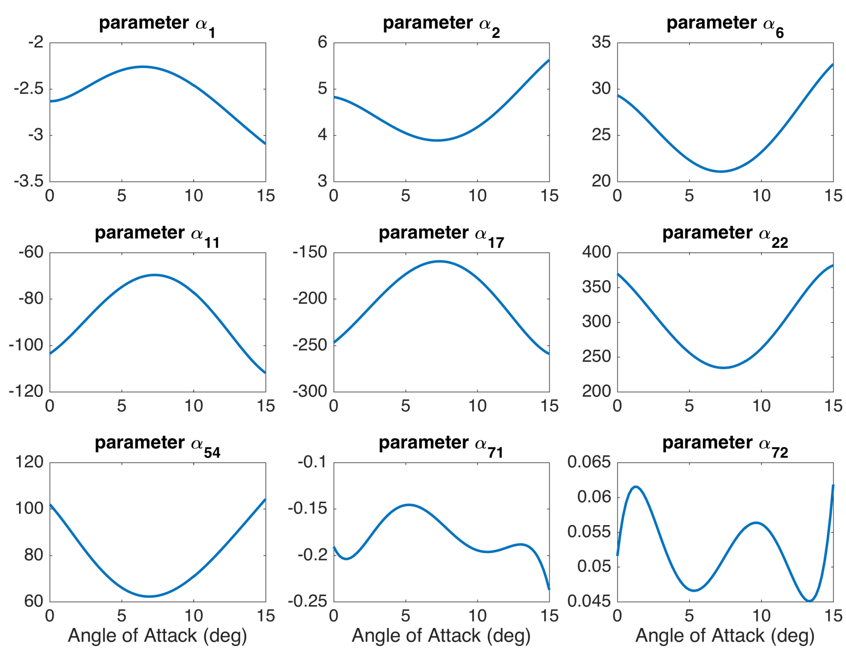

Figure 10. Indicative VFP-AR$(72)_{24}$ model parameters versus angle of attack for a set airspeed $k^1 = 15$ m/s.

phenomenon. Via the use of such a global VFP model it is possible to improve the aircraft control in order to suppress, minimize, and even predict dynamic flutter via appropriate real-time monitoring techniques.

Indicative AR parameters of the VFP-AR$(72)_{24}$ model are depicted in Figure 10 as functions of the angel of attack for a constant airspeed of 15 m/s. However, as previously mentioned, the VFP model parameters are explicit functions of both the airspeed and the angle of attack based on the selected functional subspace and the estimated coefficients of projections. Towards this end, Figure 11 presents indicative VFP-AR$(72)_{24}$ model parameters as functions of both airspeed and angel of attack.

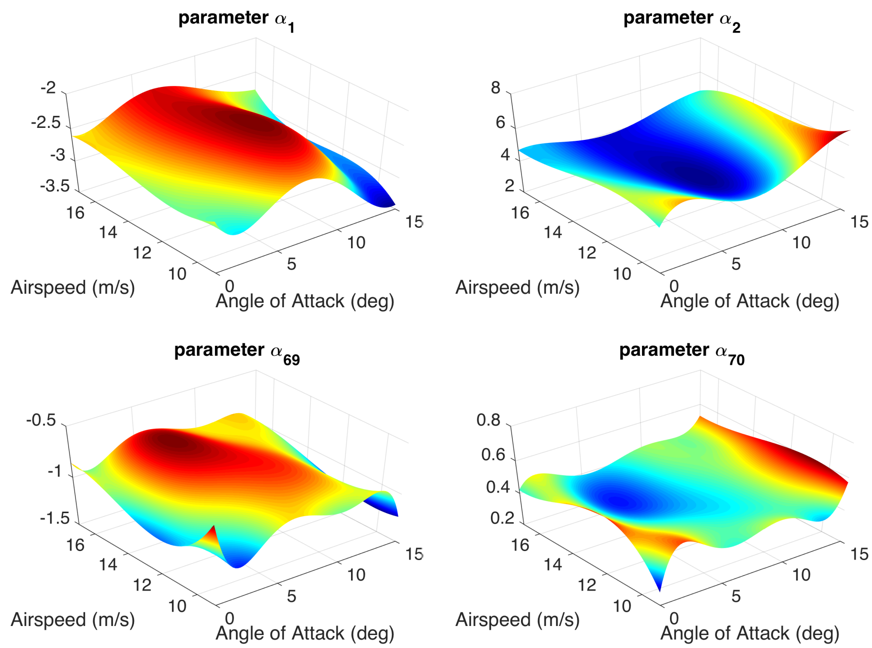

Figure 11. Indicative VFP-AR$(72)_{24}$ model parameters as function of airspeed and angle of attack.

6. CONCLUDING REMARKS

The objective of this work was to outline the main design, fabrication, and data analysis challenges of a bio-inspired self-sensing intelligent composite UAV wing with state sensing and awareness capabilities. The embedded bio-inspired stretchable sensor networks consisting of piezoelectric, strain gauges, and resistive temperature detectors enabled the identification of the coupled structural and aerodynamic properties under varying operating conditions and uncertainties. Piezoelectric sensors were used to sense the vibration of the wing in order to identify the coupled airflow-structural dynamics. Special emphasis was given to the wind tunnel experimental assessment under various flight (operating) conditions defined by multiple airspeeds and angles of attack. A novel modeling approach based on the recently introduced Vector-dependent Functionally Pooled (VFP) model structure was employed for the stochastic identification of the global coupled airflow-structural dynamics of the wing. The obtained results demonstrated the successful integration of the micro-fabricated stretchable sensor networks with the composite materials of the wing, as well as the effectiveness of the stochastic VFP-based "global" identification approach, proving their integration potential for the next generation of "fly-by-feel" aerial vehicles.

ACKNOWLEDGMENTS

This research was supported by the U.S. Air Force Office of Scientific Research (AFOSR) Multidisciplinary University Research Initiative (MURI) program under grant FA9550-09-1-0677 with Program Manager Byung-Lip (Les) Lee. The authors the contribution of Dr. Jun Wu and Dr. Shaobo Liu in the wind tunnel experimental procedure. Finally, the authors would like to acknowledge the support of Dr. Lester Su and Prof. John Eaton in the wind tunnel facility at Stanford University.

REFERENCES

[1] Lanzara, G., Salowitz, N., Guo, Z., and Chang, F.-K., "A spider-web-like highly expandable sensor network for multifunctional materials," *Advanced Materials* **22**(41), 4643–4648 (2010).

[2] Salowitz, N., Guo, Z., Li, Y.-H., Kim, K., Lanzara, G., and Chang, F.-K., "Bio-inspired stretchable network-based intelligent composites," *Journal of Composite Materials* **47**(1), 97–106 (2013).

[3] Salowitz, N., Guo, Z., Roy, S., Nardari, R., Li, Y.-H., Kim, S.-J., Kopsaftopoulos, F., and Chang, F.-K., "Recent advancements and vision toward stretchable bio-inspired networks for intelligent structures," *Structural Health Monitoring* **13**(6), 609–620 (2014).

[4] Kopsaftopoulos, F., Nardari, R., Li, Y.-H., and Chang, F.-K., "Experimental identification of structural dynamics and aeroelastic properties of a self-sensing smart composite wing," in [*Proceedings of the 10th International Workshop on Structural Health Monitoring (IWSHM)*], Chang, F.-K. and Kopsaftopoulos, F., eds. (September 2015).

[5] Holmes, M., "Global carbon fibre market remains on upward trend," *Reinforced Plastics* **58**(6), 38–45 (2014).

[6] Larrosa, C., Lonkar, K., and Chang, F.-K., "In situ damage classification for composite laminates using gaussian discriminant analysis," *Structural Health Monitoring* **13**(2), 190–204 (2014).

[7] Ihn, J. and Chang, F.-K., "Detection and monitoring of hidden fatigue crack growth using a built-in piezoelectric sensor/actuator network, part i: Diagnostics," *Smart Materials and Structures* **13**, 609–620 (2004).

[8] Ihn, J. and Chang, F.-K., "Detection and monitoring of hidden fatigue crack growth using a built-in piezoelectric sensor/actuator network, part ii: Validation through riveted joints and repair patches," *Smart Materials and Structures* **13**, 621–630 (2004).

[9] Ihn, J. and Chang, F.-K., "Pitch-catch active sensing methods in structural health monitoring for aircraft structures," *Structural Health Monitoring* **7**(1), 5–19 (2008).

[10] Janapati, V., Kopsaftopoulos, F., Li, F., Lee, S., and Chang, F.-K., "Damage detection sensitivity characterization of acousto-ultrasound-based structural health monitoring techniques," *Structural Health Monitoring* **15**(2), 143–161 (2016).

[11] Kopsaftopoulos, F. P., *Advanced Functional and Sequential Statistical Time Series Methods for Damage Diagnosis in Mechanical Structures*, PhD thesis, Department of Mechanical Engineering & Aeronautics, University of Patras, Patras, Greece (January 2012).

[12] Kopsaftopoulos, F. P. and Fassois, S. D., "Vector-dependent functionally pooled ARX models for the identification of systems under multiple operating conditions," in [*Proceedings of the 16th IFAC Symposium on System Identification, (SYSID)*], (July 2012).

[13] Sakellariou, J. S. and Fassois, S. D., "Functionally pooled models for the global identification of stochastic systems under different pseudo-static operating conditions," *Mechanical Systems and Signal Processing* **72-73**, 785807 (2016).

[14] Guo, Z., Kim, K., Lanzara, G., Salowitz, N., Peumans, P., and F.-K.Chang, "Bio-inspiredsmart skin based on expandable network," in [*Proceedings of the 8th International Workshop on Structural Health Monitoring 2011 Condition Based Maintenance and Intelligent Structures*], Chang, F.-K., ed. (September 2011).

[15] Salowitz, N., Guo, Z., Kim, S.-J., Li, Y.-H., Lanzara, G., and Chang, F.-K., "Screen-printed piezoceramic actuators/sensors microfabricated on organic films and stretchable networks," in [*Proceedings of the 9th International Workshop on Structural Health Monitoring 2013*], Chang, F.-K., ed. (September 2013).

[16] Z.Guo, *Robust Design And Fabrication Of Highly Stretchable Sensor Networks For The Creation Of Intelligent Materials*, PhD thesis, Department of Aeronautics and Astronautics, Stanford University (2014).

[17] Salowitz, N., Guo, Z., Roy, S., Nardari, R., Li, Y.-H., Kim, S., Kopsaftopoulos, F., and Chang, F.-K., "A vision on stretchable bio-inspired networks for intelligent structures," in [*Proceedings of the 9th International Workshop on Structural Health Monitoring 2013*], Chang, F.-K., ed. (September 2013).

[18] Ljung, L., [*System Identification: Theory for the User*], Prentice–Hall, 2nd ed. (1999).

[19] Söderström, T. and Stoica, P., [*System Identification*], Prentice–Hall (1989).

[20] Fassois, S. D., "Parametric identification of vibrating structures," in [*Encyclopedia of Vibration*], Braun, S., Ewins, D., and Rao, S., eds., 673–685, Academic Press (2001).

[21] Bernstein, D., [*Matrix Mathematics*], Princeton University Press (2005).

[22] Greene, W. H., [*Econometric Analysis*], Prentice–Hall, 5th ed. (2003).

[23] Drela, M. and Youngren, H., "XFOIL." http://web.mit.edu/drela/Public/web/xfoil/.

[24] Kopsaftopoulos, F. P. and Fassois, S. D., "A functional model based statistical time series method for vibration based damage detection, localization, and magnitude estimation," *Mechanical Systems and Signal Processing* **39**, 143–161 (2013).